Journal of Pharmaceuticals and Natural Sciences

B-CRETA Publisher
Pharma Insight Solutions

Article

In Silico Molecular Docking of *Murraya koenigii* (L.) Spreng. Metabolites against the Androgen Receptor

Nayla Shaffa Mardhiya [1], Muhammad Nahrawi Udharaja [2], Viviana Idris [3], Iswahyudi [2*]

[1] Faculty of Pharmacy, Universitas Mulawarman, Samarinda, East Kalimantan, Indonesia
[2] Research and Development Laboratory, PT. Borneo Riseta Naturafarm, Kutai Kertanegara, East Kalimantan, Indonesia
[3] UPTD Pusat Kesehatan Masyarakat (Puskesmas) Sidomulyo, Dinas Kesehatan Kota Samarinda, Samarinda, Kalimantan Timur, Indonesia
* Correspondence: iswahyudifarm@gmail.com

Citation: Mardhiya, N.S.; Udharaja, M.N.; Idris, V.; Iswahyudi. In Silico Molecular Docking of *Murraya koenigii* (L.) Spreng. Metabolites against the Androgen Receptor. J Pham Nat Sci 2026, 3(2), 89-101. https://doi.org/10.70392/jpns.v3i2.53

Academic Editor: Ratna Surya Alwi, Ph.D

Received: August 14th, 2026
Revised: August 24th, 2026
Accepted: August 28th, 2026

Publisher's Note: B-CRETA publisher stays neutral with regard to jurisdictional claims in published maps and institutional affiliations.

Abstract

Background: Prostate cancer remains a critical global health challenge heavily mediated by androgen receptor (AR) signaling. Secondary metabolites from *Murraya koenigii* (L.) Spreng., particularly carbazole alkaloids, possess diverse anticancer properties, yet their potential to target the AR ligand-binding domain (LBD) remains unexplored. Objective: This study evaluated the binding affinity, active site interaction modes, and ADME/drug-likeness profiles of 20 *M. koenigii* metabolites against the AR LBD *in silico*. Methods: Structure-based molecular docking was performed using AutoDock4 against AR LBD (PDB ID: 3B67), validated by redocking the co-crystallized ligand SARM C-23. Physicochemical, pharmacokinetic, and drug-likeness profiles were predicted using SwissADME. Results: Redocking validated the protocol with an RMSD of 0.77 Å. Nine metabolites exhibited superior predicted binding energies (ΔG < -9.52 kcal/mol) compared to SARM C-23. While *mahanimbine* displayed the highest affinity (ΔG = -11.48 kcal/mol), it violated drug-likeness parameters. Conversely, *O-methylmurrayamine* demonstrated a well-balanced profile with a strong binding affinity ((ΔG = -10.03 kcal.mol; Ki = 45.45 nM), key interactions with essential hydrophobic residues (LEU704, TRP741, MET742, MET745), and zero violations across five drug-likeness rules. Conclusion: *O-methylmurrayamine* represents a promising lead scaffold for AR-targeted therapy warranting further *in vitro* and *in vivo* validation.

Keywords: *Murraya koenigii*; androgen receptor; molecular docking; carbazole alkaloids; AutoDock4; SwissADME; prostate cancer

1. INTRODUCTION

Prostate cancer is one of the most frequently diagnosed malignancies among men worldwide and is a major public-health problem. The GLOBOCAN 2020 data indicating approximately 1.4 million new prostate cancer cases globally, with prostate cancer ranked among the leading cancers in Indonesian men [1,2]. Although several therapeutic strategies are available, disease progression and recurrence remain closely associated with persistent androgen receptor (AR) signaling.

Androgen deprivation therapy, androgen-synthesis inhibition, chemotherapy, and other systemic approaches therefore remain important components of prostate-cancer management [3].

The androgen receptor, encoded by the AR gene on the X chromosome, is a member of the nuclear receptor superfamily. It contains an N-terminal transactivation domain, a DNA-binding domain, a hinge region, and a C-terminal ligand-binding domain (LBD). Binding of testosterone or dihydrotestosterone to the LBD promotes receptor activation and transcriptional regulation of androgen-responsive genes. Alterations in androgen synthesis, AR amplification, receptor mutation, and generation of splice variants contribute to therapeutic resistance in advanced prostate cancer [4,5]. Consequently, disruption of androgen–AR signaling through competitive occupation of the LBD remains a rational strategy for identifying new anti-prostate-cancer agents.

Natural products provide a chemically diverse source for ligand discovery. *Murraya koenigii* (L.) Spreng., commonly known as curry leaf or salam koja, is an aromatic plant belonging to the Rutaceae family. The plant is traditionally used as a culinary spice and is distributed widely in South and Southeast Asia, including Indonesia [6–8]. Phytochemical investigations have identified numerous secondary metabolites from different plant parts, including carbazole alkaloids, terpenoids, flavonoids, phenolics, carotenoids, and other constituents. Reported bioactive compounds include mahanine, mahanimbine, isomahanine, koenimbine, girinimbine, pyrayafoline D, murrayafoline, murrayazoline, koenoline, O-methylmurrayamine, murrayanine, and related metabolites [6,7].

Pharmacological studies summarized in the source reference indicate that *M. koenigii* and its constituents have antioxidant, anti-inflammatory, antimicrobial, hepatoprotective, neuroprotective, and anticancer activities [6–8]. In particular, mahanine, girinimbine, and koenimbine have been associated with anticancer effects in previous investigations [6–8]. Nevertheless, evidence in the source material does not establish whether these metabolites can interact directly with the androgen receptor binding pocket. This represents a specific mechanistic gap that can be addressed initially using structure-based computational screening.

Molecular docking is a computational approach for predicting the preferred orientation of a ligand within a protein binding site and estimating its binding affinity. The approach can reduce the number of compounds requiring experimental screening and can provide a structural rationale for ligand–protein recognition [9–12]. In the present study, oriented docking was selected because the binding region of the androgen receptor was defined from the experimentally resolved receptor–ligand structure. AutoDock4 with a Lamarckian Genetic Algorithm was used for docking, while Discovery Studio Visualizer was used to inspect protein–ligand interactions. The docking protocol was validated by redocking the native ligand, and the resulting candidates were subsequently evaluated for physicochemical properties, lipophilicity, solubility, pharmacokinetic descriptors, and drug-likeness using SwissADME.

The novelty of this work is the integrated computational assessment of a set of 20 secondary metabolites reported from *M. koenigii* against the androgen receptor, followed by interaction profiling and preliminary drug-likeness assessment of the strongest docking candidates. The study aimed to (i) identify *M. koenigii* metabolites with favorable predicted binding to the androgen receptor, (ii) characterize the residues and interaction patterns involved in binding, and (iii) determine which high-affinity candidates show comparatively favorable predicted physicochemical and pharmacokinetic properties.

2. MATERIALS AND METHODS

2.1. Material

The molecular materials comprised the androgen receptor structure and 20 secondary metabolites reported from *M. koenigii* including mahanine, mahanimbine, isomahanine, koenimbine, girinimbine, isolongifolene, pyrayafoline D, murrayafoline, murrayazoline, koenoline, 9-formyl-3-methylcarbazole, O-methylmurrayamine, koenine, koenigine, mukonicine, mahanimbinine, murrayacinine, mahanimboline, mukoeic acid, and murrayanine [6,7]. The receptor structure and native ligand were obtained from the RCSB Protein Data Bank using PDB ID 3B67.

2.2. Instrument

Computational work was performed on a computer. AutoDock Tools 1.5.7/AutoDock4 was used for receptor and ligand preparation and molecular docking; ChemDraw and Chem3D Pro were used to generate and minimize ligand structures; Biovia Discovery Studio Visualizer was used for interaction analysis; and SwissADME was used to estimate physicochemical properties, lipophilicity, solubility, pharmacokinetic descriptors, and drug-likeness.

2.3. Method

2.3.1. Protein and Native-Ligand Preparation

The receptor and native ligand were separated using AutoDock Tools [10]. Water molecules were removed to reduce the computational burden, after which hydrogen atoms were added during receptor/ligand preparation. The prepared receptor and ligand were converted to PDBQT format. The docking region was defined around the binding site of the native ligand.

2.3.2. Ligand Preparation

Two-dimensional structures of the 20 *M. koenigii* metabolites were prepared using ChemDraw and converted to three-dimensional structures using Chem3D Pro [13]. Geometry minimization was performed using the MMFF94 force field, and the resulting structures were saved in PDB format before conversion to the docking-compatible format.

2.3.3. Docking Protocol and Validation

To define the search space, a grid box centred on the co-crystallized ligand (SARM C-23) binding pocket was generated with dimensions of 34 x 34 x 34 points, a grid spacing of 0.375 Å, and centre coordinates set at x = 27.291, y = 3.651, and z = 7.321. Method validation was performed by redocking SARM C-23 into the AR active site using 100 docking runs via the Lamarckian Genetic Algorithm (LGA). A root-mean-square deviation (RMSD) threshold of <2.0 Å between the re-docked pose and the native crystal orientation was set as the validation criterion.

2.3.4. Docking-data Analysis

Docking results were evaluated descriptively using predicted binding free energy (ΔG), predicted inhibition constant (Ki), and the identity of interacting amino-acid residues. More negative ΔG values and lower Ki values were interpreted as indicators of stronger predicted affinity relative to the native ligand. The binding-site interactions were subsequently visualized with Biovia Discovery Studio Visualizer. Particular attention was given to hydrogen bonds and hydrophobic interactions involving residues located within the native-ligand binding region.

2.3.5. In Silico ADME and Drug-likeness Analysis

The nine metabolites with more favorable docking values than the native ligand were subjected to SwissADME analysis [14]. The assessed descriptors included molecular weight, heavy atoms, aromatic heavy atoms, fraction sp3, rotatable bonds, hydrogen-bond acceptors and donors, topological polar surface area (TPSA), XLOGP3, WLOGP, MLOGP, ESOL/Ali/SILICOS-IT solubility estimates, gastrointestinal absorption, blood–brain barrier penetration, P-glycoprotein substrate status, cytochrome P450 inhibition predictions, skin permeability (Log Kp), and drug-likeness according to Lipinski, Ghose, Veber, Egan, and Muegge models [15,16].

3. RESULT AND DISCUSSION

3.1. Validation of The Molecular Docking Protocol

Redocking of the co-crystallized ligand SARM C-23 into the AR LBD yielded an RMSD of 0.77 Å, well below the standard 2.0 Å threshold, confirming that the docking parameters reliably reproduce the experimental binding mode (Figure 1). The redocked pose was therefore considered sufficiently similar to the experimentally observed native-ligand orientation to support subsequent screening. The corresponding predicted binding energy of the native ligand was −9.52 kcal/mol and its predicted Ki was 104.57 nM. This validation step is essential because comparison of test-ligand docking

scores is meaningful only when the selected search space and docking parameters can reproduce the reference binding mode with acceptable deviation [10,11].

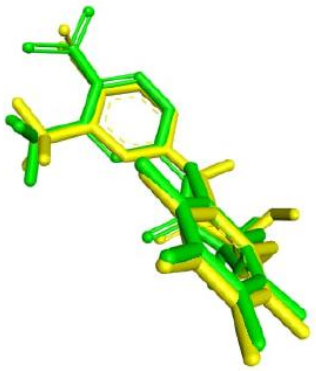

Figure 1. Validation of the molecular docking protocol via a redocking process using the original SARM C-23 ligand (the initial ligand is shown in yellow and the docking result in green), with an RMSD value of 0.77 Å, which is below the specified acceptance criterion of 2 Å.

Table 1 summarizes the predicted docking scores for the native ligand and the 20 *M. koenigii* metabolites. Nine metabolites displayed more negative ΔG and lower Ki than SARM C-23. Based on Table 1, of the 20 screened metabolites, nine compounds demonstrated predicted binding energies more favorable than SARM C-23 (ΔG = -9.52 kcal/mol; Ki = 105.31 nM). *Mahanimbine* exhibited the lowest binding energy (ΔG = -11.48 kcal/mol), followed by *koenimbine* (ΔG = -10.82 kcal/mol) and *girinimbine* (ΔG = -10.41 kcal/mol). Conversely, *murrayafoline* yielded a positive binding energy (ΔG = +4.42 kcal/mol), indicating unfavorable binding due to severe steric hindrance within the hydrophobic cavity.

Table 1. Predicted binding energy and inhibition constant of *M. koenigii* metabolites against the androgen receptor (PDB ID 3B67).

Ligand	ΔG (kcal/mol)	Estimated Ki
SARM C-23 (native)	−9.52	104.57 nM
Mahanine	−11.30	5.17 nM
Mahanimbine	−11.48	3.84 nM
Isomahanine	−11.25	5.64 nM
Koenimbine	−9.48	112.42 nM
Girinimbine	−9.50	108.39 nM
Isolongifolene	−7.86	1740 nM
Pyrayafoline D	−10.92	9.92 nM
Murrayafoline	+4.42	N/A
Murrayazoline	−10.46	21.57 nM
Koenoline	−7.57	2,83 μM
9-formyl-3-methylcarbazole	−7.54	3,01 μM
O-Methylmurrayamine	−10.03	44.60 nM
Koenine	−8.95	276.96 nM
Koenigine	−8.85	327.84 nM
Mukonicine	−9.13	203.80 nM
Mahanimbinine	−10.34	26.32 nM
Murrayacinine	−10.76	13.07 nM
Mahanimboline	−11.40	4.43 nM
Mukoeic acid	−7.30	4,480 μM
Murrayanine	−8.01	1340 nM

The binding energy value indicates the strength of the energy interaction between the ligand and the receptor. The lower the binding energy value, the stronger the bond formed between the ligand and the receptor. The inhibition constant, meanwhile, is a value that indicates the resistance to interaction between the ligand and the receptor. The smaller the inhibition constant, the less resistance there is to the ligand interacting with or binding to the receptor, thereby increasing the ligand's affinity for the receptor.

3.2. Docking Affinity of M. koenigii Metabolites

Among the screened metabolites, mahanimbine showed the most favorable predicted docking score (−11.48 kcal/mol; Ki 3.84 nM), followed by mahanimboline (−11.40 kcal/mol; 4.43 nM), mahanine (−11.30 kcal/mol; 5.17 nM), and isomahanine (−11.25 kcal/mol; 5.64 nM). Pyrayafoline D, murrayacinine, murrayazoline, mahanimbinine, and O-methylmurrayamine also showed more favorable predicted affinity than the native ligand. In contrast, several metabolites displayed weaker predicted affinity, while murrayafoline produced a positive ΔG (+4.42 kcal/mol) in the reported docking output and therefore did not show a favorable predicted interaction under the selected conditions (as shown in figure 2).

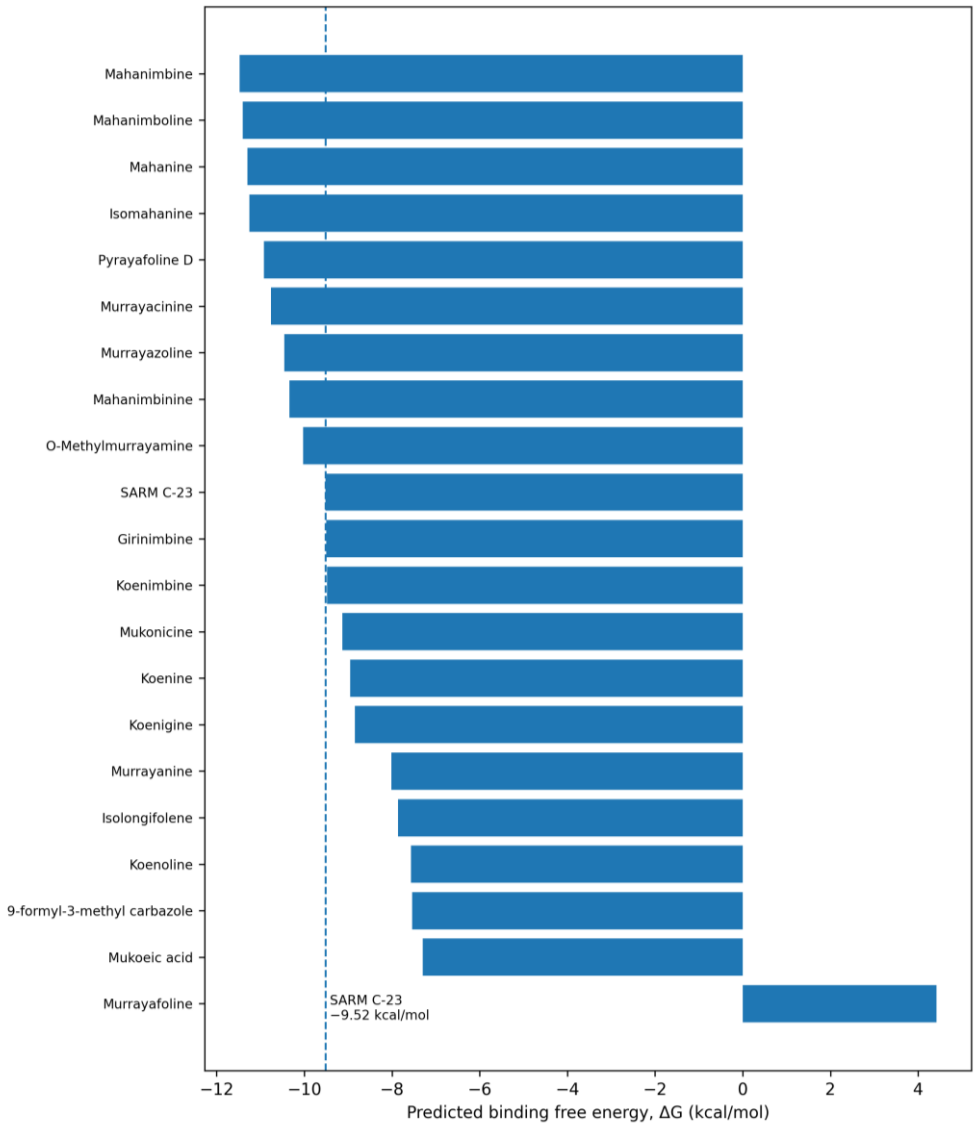

Figure 2. Predicted binding free energies (ΔG) of the reported *M. koenigii* metabolites against the androgen receptor. The dashed line denotes the native-ligand value of −9.52 kcal/mol.

The nine high-ranking compounds are chemically related to the diverse carbazole-rich phytochemistry of *M. koenigii*. Their stronger predicted binding than SARM C-23 should, however, be interpreted as a ranking result rather than direct evidence of receptor inhibition. Docking scores are approximations generated by a scoring function and do not fully account for protein flexibility, solvent effects, entropic contributions, receptor conformational ensembles, or cellular pharmacology. Thus, the present results are most appropriately considered a prioritization step for experimental validation rather than proof of anticancer activity [10,17,18].

The predicted Ki values were consistent with the ΔG ranking: compounds with the most negative binding energies generally showed the lowest predicted Ki. This concordance strengthens the internal interpretation of the docking screen. The results also indicate that structural similarity alone is insufficient to predict affinity, because compounds within the same broad phytochemical group produced substantially different docking scores. The orientation and complementarity of each ligand within the binding pocket therefore appear to be important determinants of predicted affinity.

3.3. Binding-site Interaction Profile

The interaction analysis was further supported by the complete residue profiles presented in Table 2. While Figure 3B summarizes the residues shared between the selected metabolites and the native-ligand interaction environment, Table 2 demonstrates that each compound also interacted with additional residues surrounding the androgen receptor binding cavity. Therefore, the interaction heatmap should be interpreted as a visualization of residue overlap rather than a complete representation of all receptor–ligand contacts.

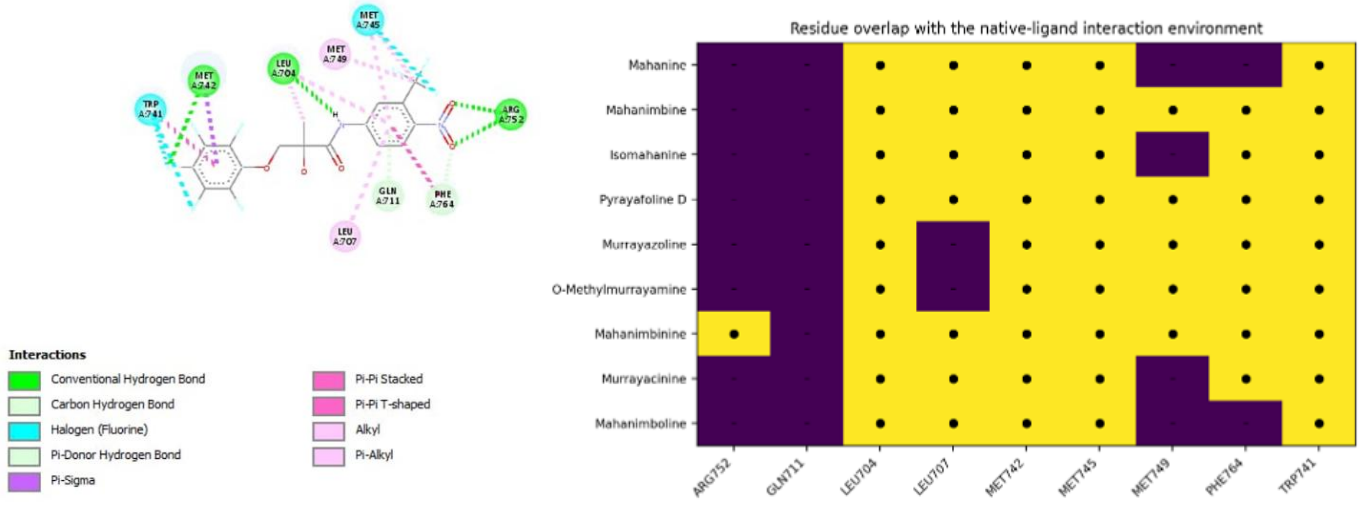

A B

Figure 3. Comparative interaction profile of the native ligand and selected high-affinity *Murraya koenigii* metabolites within the androgen receptor binding site. (A) Two-dimensional interaction map of the native ligand and (B) residue overlap analysis between the native ligand and nine selected metabolites.

The native ligand interacted with ARG752, GLN711, LEU704, LEU707, MET742, MET745, MET749, PHE764, and TRP741. Among these residues, LEU704, LEU707, MET742, MET745, MET749, PHE764, and TRP741 were frequently shared by the selected high-affinity metabolites (Figure 3B). This pattern indicates that the metabolites were predicted to occupy a binding environment overlapping substantially with that of the native ligand.

However, Table 2 shows that the candidate metabolites also established interactions with residues not observed in the native-ligand profile, including LEU873, MET780, MET787, MET895, HIS874, ILE898, ILE899, PHE876, PHE891, THR877, VAL746, and VAL903. These additional contacts suggest that individual metabolites may adopt distinct

orientations within the receptor cavity while maintaining interactions with a common core of the native-ligand binding environment.

Table 2. Predicted interacting residues of the native ligand and selected high-affinity *M. koenigii* metabolites within the androgen receptor binding pocket.

Ligand	**Interacting Active Site Residues**
Native ligand	ARG_{752}, GLN711, LEU704, LEU707, MET742, MET745, MET749, PHE764, TRP741
Mahanine	LEU704, LEU707, LEU873, MET742, MET745, MET780, MET895, PHE876, TRP741
Mahanimbine	HIS874, LEU704, LEU707, MET742, MET745, MET749, MET895, PHE764, TRP741, VAL903
Isomahanine	LEU704, LEU707, LEU873, MET742, MET745, MET780, MET895, PHE764, PHE876, TRP741
Pyrayafoline D	HIS874, ILE898, LEU704, LEU707, LEU873, MET742, MET745, MET749, MET787, PHE764, TRP741, VAL746, VAL903
Murrayazoline	LEU704, LEU873, MET742, MET745, MET749, MET780, MET787, MET895, PHE764, TRP741, VAL746
O-Methylmurrayamine	HIS874, ILE898, ILE899, LEU704, MET742, MET745, MET749, MET895, PHE764, PHE891, TRP741, VAL903
Mahanimbinine	ARG752, LEU704, LEU707, MET742, MET745, MET749, MET895, PHE764, TRP741
Murrayacinine	LEU704, LEU707, LEU873, MET742, MET745, MET780, MET895, PHE764, TRP741
Mahanimboline	LEU701, LEU704, LEU707, LEU873, MET742, MET745, MET780, MET895, THR877, TRP741

Interaction analysis revealed that all nine top candidates bind within the canonical androgen binding pocket. Key hydrophobic contacts were consistently formed with LEU704, TRP741, MET742, MET745, and VAL746. Notably, *O-methylmurrayamine* stabilized its complex through strong hydrophobic interactions with TRP741 and MET742, mimicking the essential binding envelope of reference AR modulators.

Among the compounds evaluated, mahanimbine showed extensive overlap with the native-ligand interaction profile, including LEU704, LEU707, MET742, MET745, MET749, PHE764, and TRP741, while simultaneously interacting with HIS874, MET895, and VAL903. This extensive interaction network may contribute to its favorable predicted binding energy of −11.48 kcal/mol. Similarly, pyrayafoline D showed a broad interaction profile involving several shared residues together with additional contacts at HIS874, ILE898, LEU873, MET787, VAL746, and VAL903.

Mahanine and isomahanine exhibited a related interaction pattern characterized by conserved contacts with LEU704, LEU707, MET742, MET745, and TRP741, accompanied by interactions with LEU873, MET780, MET895, and PHE876. Although these compounds did not reproduce all native-ligand contacts, their favorable docking energies suggest that alternative interaction networks within the same binding cavity may provide sufficient stabilization.

Interestingly, mahanimbinine was the only selected metabolite reported to retain interaction with ARG752, a residue also involved in native-ligand binding. Nevertheless, its predicted binding energy (−10.34 kcal/mol) was less favorable than that of mahanimbine and mahanimboline. This observation indicates that the number of residues shared with the native ligand does not directly determine docking affinity. Instead, predicted binding energy reflects the overall contribution of multiple factors, including interaction type, ligand orientation, conformational complementarity, and hydrophobic packing.

O-methylmurrayamine exhibited interactions with several residues shared with the native ligand, including LEU704, MET742, MET745, MET749, PHE764, and TRP741, together with additional contacts involving HIS874, ILE898, ILE899, MET895, PHE891, and VAL903. Although its predicted docking affinity was lower than that of several other candidates, its more favorable physicochemical and drug-likeness profile supports its prioritization as a balanced candidate for further investigation.

Overall, the combined interpretation of Figure 3 and Table 2 indicates that the selected *M. koenigii* metabolites do not simply replicate the interaction pattern of the native ligand. Instead, they appear to maintain interactions with a common core of residues within the androgen receptor binding environment while establishing ligand-specific contacts with neighboring residues. This observation may explain why compounds with different residue interaction profiles can nevertheless

exhibit similarly favorable predicted binding energies. Therefore, both the extent of residue overlap and the additional interaction network should be considered when interpreting docking results.

3.4. Physicochemical properties and lipophilicity

The nine high-affinity compounds exhibited molecular weights ranging from 293.36 to 349.47 g/mol, with 0–6 rotatable bonds and topological polar surface area (TPSA) values ranging from 91.38 to 110.48 Å² (Table 3). These values indicate that molecular size and conformational flexibility were not the major differentiating factors among the candidates. In contrast, substantial variation was observed in lipophilicity, hydrogen-bonding capacity, and polarity, suggesting that these parameters may contribute more importantly to their predicted pharmacokinetic behavior [16,19].

Table 3. Selected physicochemical descriptors of the nine high-affinity compounds

Compound	MW	Fraction sp3	Rotatable bonds	HBA	HBD	TPSA (Å²)	XLOGP3
Mahanine	347.45	0.30	3	2	2	110.48	6.27
Mahanimbine	331.45	0.30	3	1	1	108.45	6.63
Isomahanine	347.45	0.30	3	2	2	110.48	6.27
Pyrayafoline D	347.45	0.30	3	2	2	110.48	6.27
Murrayazoline	345.48	0.50	0	1	0	109.17	5.51
O-Methylmurrayamine	293.36	0.26	1	2	1	91.38	4.65
Mahanimbinine	335.48	0.39	6	1	1	108.69	7.00
Murrayacinine	347.45	0.26	6	2	1	109.06	5.80
Mahanimboline	349.47	0.30	6	2	2	109.80	5.45

The lipophilicity values, expressed as XLOGP3, ranged from 4.65 to 7.00. Mahanimbinine showed the highest predicted lipophilicity (XLOGP3 = 7.00), followed by mahanimbine (6.63), mahanine, isomahanine, and pyrayafoline D (6.27 each). Such relatively high lipophilicity may facilitate hydrophobic interactions within the androgen receptor (AR) binding cavity, which is consistent with the predominantly hydrophobic interaction pattern observed in the docking analysis. However, excessive lipophilicity may also become a potential limitation for aqueous solubility and overall oral drug development. Thus, the highly favorable docking scores of these compounds should be interpreted together with their physicochemical characteristics rather than considered as independent evidence of lead quality [16,20].

In contrast, O-methylmurrayamine exhibited the lowest XLOGP3 value (4.65) among the nine candidates, together with the lowest molecular weight (293.36 g/mol) and TPSA of 91.38 Å². Its relatively lower lipophilicity and smaller molecular size provide a more balanced physicochemical profile compared with several of the highly lipophilic candidates. Murrayazoline also showed a comparatively lower XLOGP3 value (5.51), although its molecular and hydrogen-bonding characteristics differed from those of O-methylmurrayamine.

The differences in physicochemical properties are further illustrated by the SwissADME bioavailability radar profiles (Figure 4). The radar evaluates six parameters related to oral bioavailability: lipophilicity (LIPO), molecular size (SIZE), polarity (POLAR), aqueous solubility (INSOLU), saturation (INSATU), and flexibility (FLEX). The pink area represents the generally favorable physicochemical space, whereas the red polygon represents the predicted profile of each compound. The nine compounds showed distinct patterns, particularly along the lipophilicity and solubility-related axes [14,19].

The radar profiles support the numerical findings in Table 3. Mahanine, mahanimbine, isomahanine, and mahanimboline displayed relatively pronounced lipophilic characteristics, whereas O-methylmurrayamine showed a comparatively more balanced distribution across the evaluated parameters. This distinction is important because the compounds were initially selected based on their predicted AR-binding affinity, but high receptor affinity alone does not necessarily translate into favorable oral drug-like properties.

Interestingly, O-methylmurrayamine illustrates the importance of integrating binding affinity with physicochemical properties. Its predicted binding energy of −10.03 kcal/mol was less favorable than those of mahanimbine (−11.48 kcal/mol), mahanimboline (−11.40 kcal/mol), mahanine (−11.30 kcal/mol), and several other candidates. Nevertheless, O-

methylmurrayamine showed the lowest XLOGP3, relatively low molecular weight, and a comparatively balanced bioavailability radar. Therefore, although it may not represent the strongest AR binder computationally, it may represent a more balanced starting point for further lead optimization.

Figure 4. Predicted bioavailability radar profiles of the nine high-affinity *M. koenigii* metabolites.

This finding also illustrates an important principle in computational drug discovery: the best docking score does not necessarily identify the best drug candidate. Docking primarily provides an estimate of ligand–receptor interaction favorability, whereas physicochemical and ADME properties provide complementary information about whether a compound possesses characteristics compatible with further drug development. Accordingly, the present study prioritized candidates by considering both AR-binding affinity and predicted drug-likeness [10,14,16,19].

Taken together, the combined analysis of docking affinity, physicochemical descriptors, and bioavailability radar suggests that the nine metabolites can be differentiated into candidates with very strong predicted AR binding but greater physicochemical liabilities and candidates with a more balanced overall profile. O-methylmurrayamine falls into the latter category

and therefore emerges as a particularly interesting candidate for subsequent experimental evaluation. Nevertheless, these predictions do not establish actual oral bioavailability, solubility, permeability, or pharmacokinetic exposure. Experimental studies are required to determine whether the predicted physicochemical advantages translate into favorable biological and pharmacokinetic behavior.

3.5. Solubility, Pharmacokinetics, and Drug-likeness

Predicted solubility and pharmacokinetic properties provided further differentiation among the nine high-affinity metabolites (Table 3). The ESOL model predicted relatively poor solubility for most compounds, whereas murrayazoline, O-methylmurrayamine, murrayacinine, and mahanimboline showed comparatively higher predicted solubility. However, the Ali and SILICOS-IT models generally predicted lower solubility, indicating that the solubility estimates were model-dependent. O-methylmurrayamine showed the most favorable predicted solubility according to ESOL (Log S = −4.96), although SILICOS-IT predicted poor solubility (−6.33) [20].

The predicted pharmacokinetic profiles also varied among the candidates. Most compounds showed high predicted GI absorption, while murrayazoline and mahanimbinine were predicted to have low GI absorption. Several compounds were predicted as substrates of P-glycoprotein and inhibitors of multiple CYP isoforms, suggesting potential efflux and metabolic liabilities. O-methylmurrayamine, despite its high predicted GI absorption, was predicted to be a P-gp substrate and inhibitor of several CYP enzymes, indicating that its pharmacokinetic profile should not be considered unequivocally favorable [14,21].

Drug-likeness analysis using Lipinski, Ghose, Veber, Egan, and Muegge criteria further differentiated the candidates (Figure 5). O-methylmurrayamine was the only compound without violations across all five rule sets, whereas mahanimboline showed only one violation under the Muegge rule. Most of the other compounds exhibited one violation in several models [16,21-23].

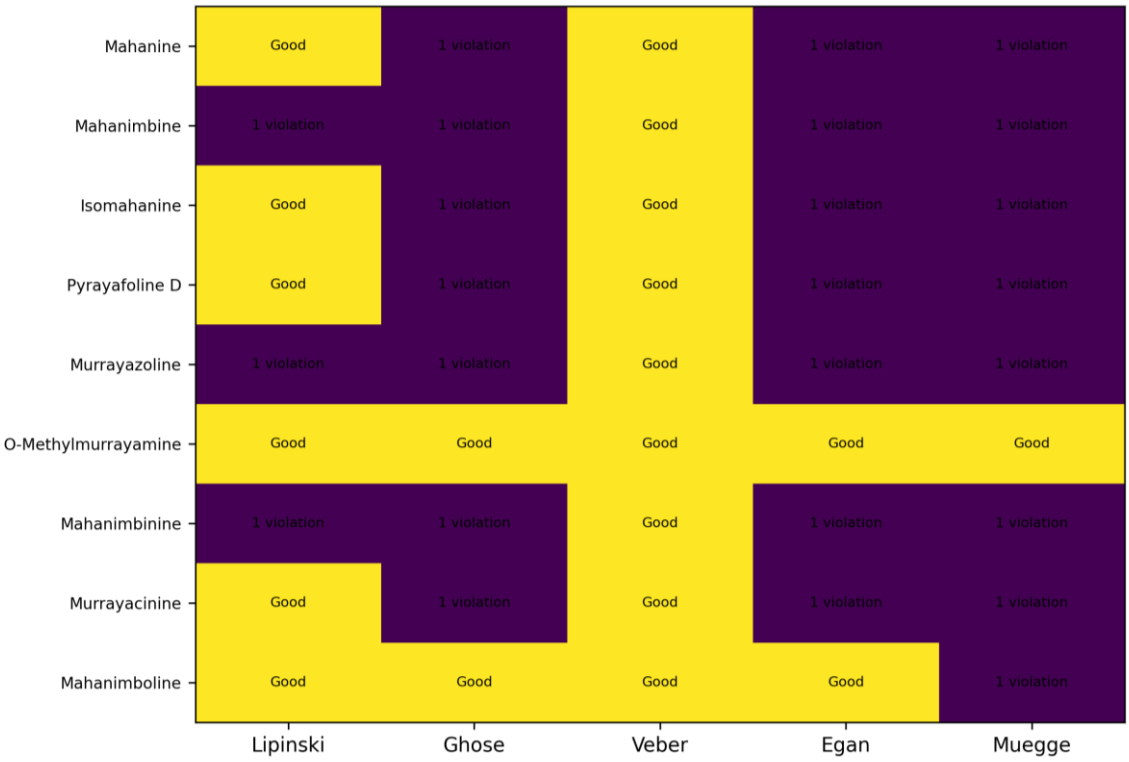

Figure 5. Drug-likeness profiles of the nine high-affinity compounds according to Lipinski, Ghose, Veber, Egan, and Muegge criteria

Taken together, these findings indicate that the strongest predicted AR binders do not necessarily possess the most favorable developability profiles. Mahanimbine showed the most favorable docking affinity, whereas O-methylmurrayamine exhibited the most balanced drug-likeness profile. Therefore, O-methylmurrayamine may be prioritized as a computationally balanced lead, while its predicted P-gp substrate status and CYP inhibition liabilities warrant further pharmacokinetic and experimental validation [14,16,19,23].

3.6. Pharmacological Implication and Limitation

The present computational screen provides a rational basis for prioritizing *M. koenigii* metabolites for experimental investigation of AR signaling. The most promising docking candidates share a common receptor region with the reference ligand and show favorable predicted binding energies. This is relevant because AR signaling is a central driver of prostate-cancer biology and natural products can offer structurally diverse scaffolds for lead discovery [4,5]. The carbazole-rich chemistry of *M. koenigii* therefore represents a useful starting point for structure-based exploration [17,18,24,25].

Several limitations should be explicitly recognized. First, molecular docking is a predictive method and cannot establish biological activity by itself. Second, the docking calculations were performed with a defined receptor structure and a fixed search region; alternative receptor conformations may alter ligand ranking. Third, the reported ADME and drug-likeness parameters are computational estimates and can differ from experimental pharmacokinetics. Fourth, the source thesis contains methodological inconsistencies in software version and PDB designation, although the reported results consistently identify PDB 3B67 as the target structure and AutoDock Tools 1.5.7 as the analysis environment [10,14].

Future work should include biochemical AR-binding assays, AR reporter assays, prostate-cancer cell-line studies, cytotoxicity/selectivity evaluation, and if activity is confirmed pharmacokinetic and in vivo studies. Additional computational analyses such as molecular dynamics simulations and MM/PBSA or MM/GBSA free-energy estimation could further refine candidate prioritization. Among the compounds examined here, O-methylmurrayamine deserves particular attention because it combines favorable docking with the most balanced predicted drug-likeness profile [10,14].

5. CONCLUSION

This *in silico* study demonstrates that carbazole alkaloids from *Murraya koenigii* can effectively bind to the Androgen Receptor ligand-binding domain. Among the 20 metabolites evaluated, *O-methylmurrayamine* emerged as the most promising lead candidate. It combines high predicted binding affinity (ΔG = -10.03 kcal/mol), essential active-site interaction profiles with key residues (LEU704, TRP741, MET742), and an impeccable ADME/drug-likeness profile with zero rule violations. While these computational findings provide a strong structural foundation, experimental *in vitro* binding assays, cellular reporter assays (to distinguish AR antagonism from agonism), and Molecular Dynamics simulations are required to validate its therapeutic potential against prostate cancer.

AUTHOR CONTRIBUTION: **Conceptualization** Nayla Shaffa Mardhiya and Iswahyudi; **methodology**, Muhammad Nahrawi Udharaja and Viviana Idris; **software**, Nayla Shaffa Mardhiya; **validation**, Viviana Idris and Iswahyudi; **formal analysis**, Muhammad Nahrawi Udharaja; **investigation**, Viviana Idris, Muhammad Nahrawi Udharaja, and Iswahyudi; **resource**, Nayla Shaffa Mardhiya and Iswahyudi; **data curation**, Viviana Idris and Muhammad Nahrawi Udharaja; **writing preparation of original draft**, Nayla Shaffa Mardhiya and Iswahyudi; **writing reviewing and editing**, Iswahyudi. All authors have read and approved the published version of the manuscript.

FUNDING: This research received no external funding.

ACKNOWLEDGMENT: The authors would like to express their gratitude to the Faculty of Pharmacy and all lecturers who provided academic guidance and support during the preparation of this review article. Appreciation is also extended

to colleagues and peers who contributed through constructive discussions and feedback. The authors acknowledge the use of various scientific databases and published literature that made this review possible.

CONFLICT OF INTEREST: The author declares no conflict of interest.

REFERENCES

1. Balakrishnan, R., Vijayraja, D., Jo, S.H., Ganesan, P., Su-Kim, I., Choi, D.K. Medicinal profile, phytochemistry, and pharmacological activities of *Murraya koenigii* and its primary bioactive compounds. *Antioxidants* **2020**, *9*(2), 101.
2. Bray, F., Ferlay, J., Soerjomataram, I., Siegel, R.L., Torre, L.A., Jemal, A. Global cancer statistics 2018: GLOBOCAN estimates of incidence and mortality worldwide for 36 cancers in 185 countries. *CA Cancer J Clin* **2018**, *68*, 394–424.
3. Lawrenti, H. Perkembangan Terapi Kanker Prostat. *Cermin Dunia Kedokteran* **2019**, *46*(8), 521–528.
4. Messner, E.A., Steele, T.M., Tsamouri, M.M., Hejazi, N., Gao, A.C., Mudryj, M., Ghosh, P.M. The androgen receptor in prostate cancer: Effect of structure, ligands and spliced variants on therapy. *Biomedicines* **2020**, *8*(10), 422.
5. Lucas-Herald, A.K., Touyz, R.M. Androgens and androgen receptors as determinants of vascular sex differences across the lifespan. *Canadian Journal of Cardiology* **2022**, *38*, 1854–1864.
6. Chauhan, B., Dedania, J., Mashru, R.C. Review on *Murraya koenigii*: Versatile role in management of human health. *World Journal of Pharmaceutical and Pharmaceutical Sciences* **2017**, *6*(3), 476–493.
7. Goel, A., Sharma, A., Kulshrestha, S. A phytopharmacological review on *Murraya koenigii*: an important medicinal plant. *International Journal of Pharmaceutical Sciences Review and Research* **2020**, *62*(2), 113–119.
8. Kumar, S.R., Loveleena, D., Godwin, S. Medicinal property of *Murraya koenigii*—a review. *International Research Journal of Biological Sciences* **2013**, *2*(9), 80–83.
9. Khaerunnisa, S.K., Suhartati, S., Awaluddin, R.A. Penelitian *In Silico* untuk Pemula. Airlangga University Press: Surabaya, Indonesia, **2023**.
10. Morris, G.M., Huey, R., Lindstrom, W., Sanner, M.F., Belew, R.K., Goodsell, D.S., Olson, A.J. AutoDock4 and AutoDockTools4: Automated docking with selective receptor flexibility. *Journal of Computational Chemistry* **2009**, *30*(16), 2785-2791.
11. Rose, P.W., Prlić, A., Altunkaya, A., Bi, C., Bradley, A.R., Christie, C.H., Di Costanzo, L., Duarte, J.M., Dutta, S., Feng, Z., Green, R.K., Goodsell, D.S., Hudson, B., Kalro, T., Lowe, R., Peisach, E., Randle, C., Rose, A.S., Shao, C., Tao, Y.P., Valasatava, Y., Voight, M., Westbrook, J.D., Woo, J., Yang, H., Young, J.Y., Zardecki, C., Berman, H.M., Burley, S.K. The RCSB Protein Data Bank: Integrative view of protein, gene and 3D structural information. *Nucleic Acids Research* **2017**, *45*, D271–D281.
12. Baroroh, U., Biotek, M., Muscifa, Z.S., Destiarani, W., Rohmatullah, F.G., Yusuf, M. Molecular interaction analysis and visualization of protein-ligand docking using Biovia Discovery Studio Visualizer. *Indonesian Journal of Computational Biology* **2023**, *2*(1), 22–30.
13. Li, Z., Wan, H., Shi, Y., Ouyang, P. Personal experience with four kinds of chemical structure drawing software: review on ChemDraw, ChemWindow, ISIS/Draw, and ChemSketch. *Journal of chemical information and computer sciences* **2004**, *44*(5), 1886-1890.
14. Daina, A., Michielin, O., Zoete, V. SwissADME: a free web tool to evaluate pharmacokinetics, drug-likeness and medicinal chemistry friendliness of small molecules. *Scientific reports* **2017**, *7*(1), 42717.
15. Jia, C.Y., Li, J.Y., Hao, G.F., Yang, G.F. A drug-likeness toolbox facilitates ADMET study in drug discovery. *Drug discovery today* **2020**, *25*(1), 248-258.
16. Lipinski, C.A., Lombardo, F., Dominy, B.W., Feeney, P.J. Experimental and computational approaches to estimate solubility and permeability in drug discovery and development settings. *Advanced Drug Delivery Reviews* **2001**, *46*(1–3):3–26.
17. Reisch, J., Goj, O., Wickramasinghe, A., Bandara Herath, H.M.T., Henkel, G. Carbazole alkaloids from seeds of *Murraya koenigii*. *Phytochemistry* **1992**, *31*(8), 2877–2879.

18. Ramsewak, R.S., Nair, M.G., Strasburg, G.M., DeWitt, D.L., Nitiss, J.L. Biologically active carbazole alkaloids from *Murraya koenigii*. *Journal of Agricultural and Food Chemistry* **1999**, *47*(2), 444–447.
19. Veber, D.F., Johnson, S.R., Cheng, H.Y., Smith, B.R., Ward, K.W., Kopple, K.D. Molecular properties that influence the oral bioavailability of drug candidates. *Journal of Medicinal Chemistry* **2002**, *45*(12), 2615–2623.
20. Delaney, J.S. ESOL: Estimating aqueous solubility directly from molecular structure. *Journal of Chemical Information and Computer Sciences* **2004**, *44*(3), 1000–1005.
21. Egan, W.J., Merz, K.M., Baldwin, J.J. Prediction of drug absorption using multivariate statistics. *Journal of Medicinal Chemistry* **2000**, *43*(21), 3867–3877.
22. Guzman-Pando, A., Ramirez-Alonso, G., Arzate-Quintana, C., Camarillo-Cisneros, J. Deep learning algorithms applied to computational chemistry. *Molecular Diversity* **2024**, *28*(4), 2375-2410.
23. Castellino, N.J., Montgomery, A.P., Danon, J.J., Kassiou, M. Late-stage functionalization for improving drug-like molecular properties. *Chemical reviews* **2023**, *123*(13), 8127-8153.
24. Jacob, A., Raj, R., Allison, D.B., Myint, Z.W. Androgen receptor signaling in prostate cancer and therapeutic strategies. *Cancers* **2021**, *13*(21), 5417
25. Westaby, D., Fenor de La Maza, M.D., Paschalis, A., Jimenez-Vacas, J.M., Welti, J., de Bono, J., Sharp, A. A new old target: androgen receptor signaling and advanced prostate cancer. *Annual Review of Pharmacology and Toxicology* **2022**, *62*, 131–153.